Eurographics Workshop on Visual Computing for Biology and Medicine (2014)
I. Viola, K. Bühler, and T. Ropinski (Editors)

Robust Cardiac Function Assessment in 4D PC-MRI Data

B. Köhler[1], U. Preim[2], M. Gutberlet[3], K. Fischbach[4] and B. Preim[1]

[1] OvGU Magdeburg, Germany, Institute for Simulation and Graphics
[2] Hospital Magdeburg, Germany
[3] Herzzentrum Leipzig, Germany
[4] University Hospital Magdeburg, Germany

Abstract

Four-dimensional phase-contrast magnetic resonance imaging (4D PC-MRI) is a relatively young image modality that allows the non-invasive acquisition of time-resolved, three-dimensional blood flow information. Stroke volumes and regurgitation fractions are two of the main measures to assess the cardiac function and severity of pathologies. The flow volumes in forward and backward direction through a plane inside the vessel are required for their quantification. Unfortunately, the calculations are highly sensitive towards the plane's angulation since orthogonally passing flow is considered. This often leads to physiologically implausible results. In this work, a robust quantification method is introduced to overcome this problem. Collaborating radiologists and cardiologists were carefully observed while estimating stroke volumes in various healthy volunteer and patient datasets with conventional quantification. This facilitated the automatization of their approach which, in turn, allows to derive statistical information about the plane angulation sensitivity. Moreover, the experts expect a continuous decrease of the stroke volume along the vessel course after a peak value above the aortic valve. Conventional methods are often unable to produce this behavior. Thus, we present a procedure to fit a function that ensures such physiologically plausible results. In addition, the technique was adapted for the robust quantification of regurgitation fractions. The performed qualitative evaluation shows the capability of our method to support diagnosis, a parameter evaluation confirms the robustness. Vortex flow was identified as main cause for quantification uncertainties.

Categories and Subject Descriptors (according to ACM CCS): I.4.9 [Computing Methodologies]: Image Processing and Computer Vision—Applications

1. Introduction

Cardiovascular diseases (CVDs) are the number one cause of death in the world [MPN11]. Their genesis and evolution depends on various factors. Recent works have shown that complex flow patterns like vortices are a strong indicator for many pathologies of the cardiovascular system [KGP*13]. Yet, when it comes to assessing the severity, quantitative measures are essential.

Four-dimensional phase-contrast magnetic resonance imaging (4D PC-MRI) is a relatively young modality that allows to gain insight into the patient-specific hemodynamics. Such time-resolved, three-dimensional flow information have a great potential to support diagnosis and the choice of appropriate treatments. Advances in recent years greatly reduced acquisition times to a few minutes and thus increased the viability for clinical routine [HSD13]. However, 4D PC-MRI acquisitions are currently mostly performed for the sole purpose of research. There is a lack of standardized, easy-to-use and (semi-)automatic approaches that increase the practical applicability [MFK*12]. Though, different research groups explore the potential of 4D PC-MRI by developing new and improving existing evaluation methods. In addition, reliability is validated via comparisons to the current 2D PC-MRI standard as well as simulated CFD data.

Two of the most important quantitative measures to assess the cardiac function are *stroke volumes* and *regurgitation fractions*. The first describes the volume of pumped blood per heartbeat, the second characterizes the percentaged back flow during diastole, which is about zero in a healthy person. Both quantifications require the flow volumes in forward and backward direction through a plane that is usually aligned orthogonally to the vessel's centerline. Unfortunately, the calculations show a high sensitivity towards the plane's angulation. Unlike 2D PC-MRI, where unsatisfying results make a whole new acquisition necessary, 4D PC-

DOI: 10.2312/vcbm.20141179

MRI datasets contain the patient's full four-dimensional flow information. This allows to easily evaluate multiple planes with different positions and angulations.
In this work, we analyzed various healthy volunteer and patient datasets in close collaboration with radiologists and cardiologists. We carefully observed their manual approach to estimate stroke volumes and regurgitation fractions while anticipating the high sensitivity towards the plane angulation. From this we derived an automatic procedure which systematically evaluates multiple angulations for one position on the vessel's centerline. The obtained statistical information facilitate to robustly determine the stroke volume and visualize the uncertainty.
If no pathologies are present, the cooperating experts expect the highest stroke volume directly above the aortic valve. From there a continuous decrease along the vessel course is assumed due to smaller vessels that branch off and supply blood to certain body regions. However, due to noise and a low spatio-temporal data resolution conventional quantification methods often produce physiologically implausible results, i.e., the stroke volume development is not monotonous. We employed the two heuristics to establish a procedure that fits a function which guarantees the desired behavior. To the best of our knowledge, there is no other work that considers the stroke volume development along the vessel's centerline. In addition, we adapted this method for the robust quantification of regurgitation fractions. Summarizing, the main contributions of this paper are:

- We automatized cardiologists' and radiologists' manual approach to determine stroke volumes despite of the calculation's high sensitivity towards the plane angulation. Derived statistical information are used to illustrate the uncertainty.
- We employed the experts' expectations about the stroke volume development along the vessel course to create a procedure that fits a physiologically plausible function.
- We put emphasis on a GPU implementation and thus provide detailed information about required data models.
- We performed an informal evaluation of selected healthy volunteer as well as patient datasets and identify potential causes for uncertainties in the discussion.

Section 2 provides basic information about 4D PC-MRI, related quantification and visualization techniques. Section 3 continues with medical background about stroke volumes and regurgitation fractions, selected cardiac pathologies, data acquisition and preprocessing. This is followed by a requirement analysis in Section 4. Section 5 explains our robust quantification method, how we establish a physiologically plausible stroke volume development and the adaption to regurgitation fractions. We present and discuss results in Section 6 and draw conclusions in Section 7.

2. Related Work

Markl et al. provide a general overview about 4D PC-MRI [MFK*12]. Recent works found good agreement with the common 2D PC-MRI standard by comparing quantitative measures like peak and mean velocities [PHL*13]. Software solutions were introduced that provide a data preprocessing pipeline [HFS*11]. Temporal maximum intensity projections (tMIP) are calculated to obtain contrast-enhanced images that support vessel segmentation [vPBB*10].
Particle animations as well as integral lines enhanced with halos and illumination are the most common techniques to visualize blood flow [MLP*10]. Illustrative [BMGS13] and other expressive visualizations [HGH*10] are used to reduce visual clutter and enhance the spatial perception. Lens-based focus-and-context visualization [GNBP11] as well as special widgets to probe the flow guided by the vascular anatomy [NJB*11] support the qualitative analysis of the highly complex 4D PC-MRI data.
Vortex flow is a strong indicator for several cardiac diseases [HWS*12]. Line predicates were used to extract such flow features [BPM*13] and the λ_2-criterion was determined as most suitable for the cardiac context [KGP*13]. Noise-robustness was improved using an orthogonal decomposition of the flow data [CBHP14].
Wall shear stress is an essential scalar measure directly obtained from blood flow simulations or indirectly approximated from 4D PC-MRI data [vOPN*14]. The calculation's high sensitivity towards low data resolutions was pointed out [PCM*14]. Stroke volumes [HSD13] and regurgitation fractions [FSS*12] are quantified to assess the cardiac function, severity of pathologies and to verify new acquisition techniques [CTK*11].

3. Medical Background

4D PC-MRI enables the time-resolved, three-dimensional acquisition of blood flow data. Such information help to comprehend the nature of various cardiovascular diseases [MPN11] and determine correlations between different qualitative features and quantitative measures.

3.1. Cardiac Function

During systole, oxygenated blood is pumped from the left ventricle through the aortic valve into the aorta while deoxygenated blood is pumped from the right ventricle through the pulmonary valve into the pulmonary artery. *Stroke volume* (SV) is the amount of pumped blood per heartbeat. Thus, it describes the difference between the antegrade (forward) and retrograde (backward) flow volume. Usually it is quantified with a plane directly above the aortic or pulmonary valve. If a valve does not close properly during diastole, blood flows back into the corresponding ventricle. The ratio between the retrograde- and sum of retrograde- and antegrade flow volume is referred to as *regurgitation fraction*

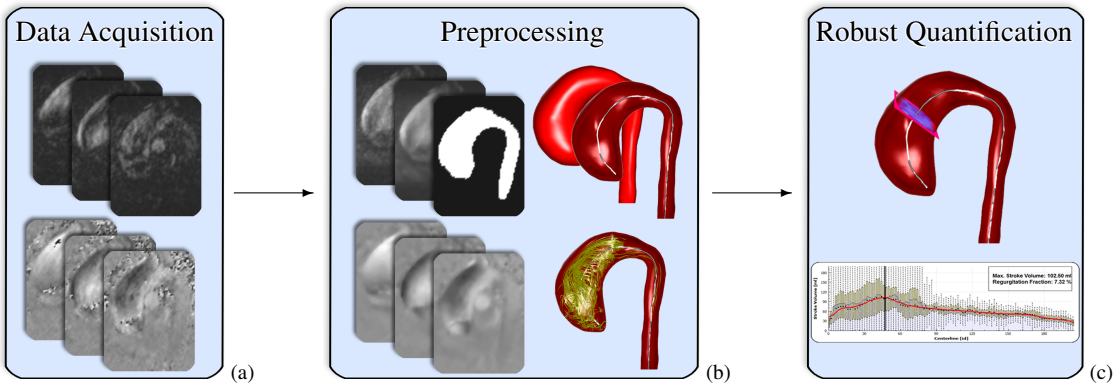

Figure 1: *(a) Each three magnitude (top) and flow images (bottom) for x-, y- and z-dimension describe the flow strength and direction, respectively. (b) Top: a segmentation is performed on a high-contrast temporal magnitude intensity projection (tMIP) of the magnitude images and used to extract the vessel mesh as well as a centerline. Bottom: vortices are extracted after the flow images were corrected. (c) Our robust stroke volume and regurgitation fraction quantification is applied.*

(RF). Even in healthy persons the valves do not always close completely. Thus, RFs below 5% are considered as unproblematic [WKS*09]. Higher percentages can lead to a valve replacement surgery if the patient shows severe symptoms.

3.2. Selected Pathologies

There is only a slight systolic helix in the aortic arch of a healthy person while the rest of the flow is typically laminar with a parabolic velocity profile. The angle between the plane normal and flow direction is essential for the SV and RF quantification. It has a potentially strong variation in vessel sections with complex flow like vortices. Thus, we explain selected pathologies that cause vortex flow and refer to [KGP*13] for additional information.

An *ectasia* denominates a slight vessel dilation up to 1.5 times the original diameter. Dilations with larger factors are called *aneurysm*. On the contrary, a *coarctation* is a pathologic narrowing. All conditions have an abnormal diameter in common. The altered vessel shape promotes the formation of vortex flow.

A healthy aortic valve consists of three leaflets that open during systole and close during diastole. *Bicuspid aortic valves (BAV)* consist of only two leaflets. This negatively affects the valve's ability to open widely, which often causes systolic vortex flow in the ascending aorta [HWS*12].

3.3. Data Acquisition and Preprocessing

A 4D PC-MRI dataset consists of each three (x, y, z) time-resolved magnitude and flow images that represent the flow strength and direction, respectively. Our datasets were acquired with a 3T Siemens Verio MR scanner. The grid size is 132 rows $\times$ 192 columns $\times$ 15 to 23 slices for each of the 14 to 21 time steps. The obtained spatial resolution is 1.77 mm $\times$ 1.77 mm $\times$ 3.5 mm with about 50 ms difference between subsequent temporal positions. The V_{ENC} parameter for the maximal expected velocity was set to 1.5 m/s. Artifacts in the phase images were reduced via eddy current correction [LHM*05] and phase unwrapping [DR04]. Figure 1 illustrates the data acquisition, preprocessing and our presented method.

A graph cut-assisted segmentation† [JSH12, LS10] is performed on a tMIP of the magnitude images. The required edge weights between nodes are specified with the exponential function $\exp(-\alpha \cdot ||\nabla I||^2)$, where I is the image intensity and α a tolerance parameter that is set to an experimentally determined default value of 1000. Morphological closing and opening is applied to the obtained binary segmentation as postprocessing.

The vessel surface is extracted via marching cubes, postprocessed with a low-pass smoothing filter [TZG96] as well as quadric decimation [Hop99] and then used to extract the centerline‡ [AEIR03].

Velocity vectors $\vec{u} \in \mathbb{R}^3$ are composed in a Runge-Kutta-4 scheme [DP80]. Each of the required samples $\vec{v} \in \mathbb{R}^3$ at the spatio-temporal position $\vec{p} = (\vec{x}, t), \vec{x} \in \mathbb{R}^3$ in the flow field $\mathbb{V}$ is calculated via quadrilinear interpolation. The temporally adjacent velocity vectors $\vec{v_{\lfloor t \rfloor}} = \mathbb{V}(\vec{x}, \lfloor t \rfloor)$ and $\vec{v_{\lceil t \rceil}} = \mathbb{V}(\vec{x}, \lceil t \rceil)$ are obtained by hardware-accelerated trilinear interpolation. $\vec{v}$ is their linear interpolation with the weight $t - \lfloor t \rfloor$. Our datasets are small enough to fit into the GPU's memory. Thus, data streaming approaches are not necessary.

4. Requirement Analysis

The automatic evaluation of different plane angulations should need only a small number of angulation samples in order to limit the computational effort. Thus, an adequate sample distribution is required. The obtained information

† GridGraph_3D_26C (GridCut)

‡ vtkMarchingCubes, vtkWindowedSincPolyDataFilter, vtkQuadricDecimation (VTK) and vmtkcenterlines (VMTK)

about the SV distribution shall be utilized to provide insight into the uncertainties, i.e., show the SV variations. A proper function has to be determined that represents the expected continuous decrease of the SV along the vessel course after a peak above the valve.
The high computational power of the GPU should be exploited. Therefore, algorithm parallelization as well as an appropriate data structure for the quantification planes are required.
Practical applicability of our method has to be ensured by avoiding unintuitive user-specified parameters. Thus, reasonable default values have to be provided. All necessary interactions should fit to the clinicians' mental model and utilize their expert knowledge.

5. Robust Cardiac Function Assessment

Carefully observing cardiologists and radiologists while estimating SVs and RFs gave insight into their usual approach. They manually alter a quantification plane's angulation repeatedly at a given position on the vessel's centerline and estimate a plausible mean value based on their experience. In the following, we present a robust SV quantification method which is an automatization of this approach. We start with a detailed description of the employed quantification plane model and provide basic information about SV calculation. We proceed with the systematic angulation sample generation and summarize the GPU-supported evaluation procedure. Afterwards, a process to fit a physiologically plausible function to the SV development along the vessel course is explained. The resulting function represents our collaborators' expectations which were employed as heuristics. The proposed method is applied to RFs in the last part.

5.1. Plane Model

A quantification plane is modeled as grid with the following components: $\vec{g} \in \mathbb{N}^2$ is a parameter that describes the number of rectangles in x- and y-dimension. $\vec{c} \in \mathbb{R}^3$ is a center position that lies on the vessel's centerline. $\vec{n} \in \mathbb{R}^3$ is the plane's normal vector, i.e. angulation, that is commonly set to the corresponding normalized centerline tangent. $\vec{n}_x$ and $\vec{n}_y \in \mathbb{R}^3$ form a local orthonormal system with $\vec{n}$. $\vec{s} \in \mathbb{R}^2$ is the size per rectangle and has to be determined by fitting the plane P to the vessel. For this purpose, the plane's intersection curve with the triangular vessel mesh is determined. Then, the maximum extents in $\vec{n}_x$- and $\vec{n}_y$-dimension are analyzed and $\vec{s}$ is set accordingly so that P is the minimum axis-aligned bounding rectangle of the vessel cross-section. Figure 2a shows an example.
These information are sufficient to calculate world coordinates for every grid point. The low memory requirements are advantageous for GPU computation.

5.2. Basic Stroke Volume Quantification

The time-dependent flow rate $fr(t)$, $t \in [0, T-1]$, where T is the number of temporal positions in dataset, is required to calculate the SV for the plane P:

$$fr(t) = s_x \cdot s_y \cdot \vec{n} \cdot \sum_{x=0}^{g_x-1} \sum_{y=0}^{g_y-1} S(P(x,y)) \cdot \mathbb{V}(P(x,y),t)$$

$$\text{with} \quad S(P(x,y)) = \begin{cases} 1, & P(x,y) \text{ inside vessel} \\ 0, & \text{else} \end{cases} \tag{1}$$

$P(x,y)$ is the grid position (x,y) transformed to world coordinates $\vec{w} \in \mathbb{R}^3$:

$$\vec{w} = \vec{c} + (s_x \cdot \vec{n}_x \cdot (x - g_x/2)) + (s_y \cdot \vec{n}_y \cdot (y - g_y/2)) \tag{2}$$

$\vec{g} = (g_x, g_y)$, $\vec{s} = (s_x, s_y)$, $\vec{c}$, $\vec{n}_x$ and $\vec{n}_y$ refer to the previous Section 5.1. $\mathbb{V}(P(x,y),t)$ is the corresponding velocity vector $\vec{u}$ in the flow field $\mathbb{V}$. The product $s_x \cdot s_y$ is the area per rectangular grid element. Since a 4D PC-MRI dataset contains one full heartbeat, $fr(t)$ is periodic. The integral of $fr(t)$ provides the SV, depicted in Figure 2c. A periodic spline fitting[§] is utilized in the implementation. The vessel segmentation is employed to realize $S(P(x,y))$. This allows to exploit hardware-accelerated 3D texture lookups on the GPU.

5.3. Plane Angulation Sample Generation

The automatic evaluation of different plane angulation samples $\vec{a}$, i.e. normal vectors, requires their systematic generation. All possible angulations form a half sphere, where the

§ spline1dbuildcatmullrom (ALGLIB)

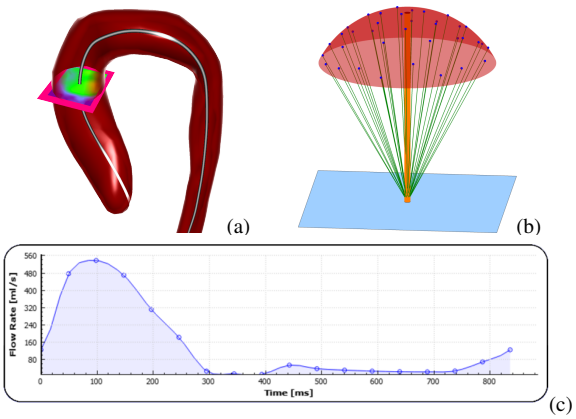

Figure 2: *(a) A quantification plane was fitted to the ascending aorta of this healthy volunteer. (b) Poisson-distributed angulation samples (green) were generated on a $\alpha = \pi/4 \mathrel{\widehat{=}} 45^o$ sphere section (red) around the plane's (blue) normal vector (orange). (c) The stroke volume is obtained as integral of the time-dependent flow rate.*

plane's original normal vector $\vec{n}$ points to the top. The maximal angle between $\vec{n}$ and $\vec{a}$ is $\alpha = \pi/2 \mathrel{\widehat{=}} 90^{\circ}$. Lower α restrict the angulation to a smaller sphere section. Thus, α describes an angulation tolerance.

The inverse cumulative distribution function (CDF) method allows to generate uniformly distributed samples on a sphere within $[\theta_1, \theta_2]$ and $[\phi_1, \phi_2]$, where θ and ϕ are longitude and latitude, respectively:

$$\theta = \operatorname{acos}(\cos\theta_1 + u \cdot (\cos\theta_2 - \cos\theta_1))$$
$$\phi = \phi_1 + v \cdot (\phi_2 - \phi_1) \tag{3}$$

u and $v \in [0,1]$ are uniformly distributed random numbers. For $\vec{n} = (0,0,1)$ the sphere section is described by $\phi_1 = 0$, $\phi_2 = 2\pi$, $\theta_1 = 0$ and $\theta_2 = \alpha \in [0, \pi/2]$. The samples are transformed from spherical coordinates $(1, \theta, \phi)$ to cartesian coordinates (x, y, z) and used to obtain the angulation sample $\vec{a} = x \cdot \vec{n}_x + y \cdot \vec{n}_y + z \cdot \vec{n}$, where $\vec{n}_x$ and $\vec{n}_y$ are part of the plane's orthonormal system (recall Section 5.1).

We create Poisson-distributed angulations A via an adapted acceptance-rejection method. Candidates are generated with Eq. 3 and added to A if the distance on the unit sphere surface to each $a \in A$ is at least $d_{\min}$. Poisson-distribution ensures that the whole sphere section is covered with few samples, which limits the computational effort. A new distribution is calculated for each plane evaluation to avoid bias.

5.4. Robust Stroke Volume Quantification

The robust SV determination for one plane is summarized in algorithm 1. The evaluation of all angulation samples provides a range of SVs with an unknown distribution and possible outliers. Thus, the median of this SV distribution seems appropriate as result.

Our collaborating cardiologists and radiologists expect a continuous decrease of the SV after a peak located above the valve. This is due to smaller vessels that branch off the main vessel and supply blood to certain regions of the body. Yet, conventional quantification, which means to evaluate only one plane that is orthogonal to the centerline, is often not

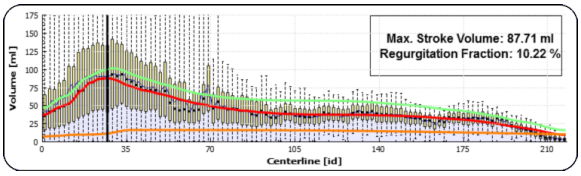

Figure 3: *The stroke volume distributions, obtained with our systematic evaluation of plane angulations for each point of the centerline, are shown as box plots, where the yellow boxes represent the interquartile ranges. The fitted, physiologically plausible functions for the stroke volume as well as antegrade and retrograde flow volume are shown in red, green and orange, respectively.* 10.22% *RF were determined at the* 87.71 *ml SV peak location (black vertical line) in this patient with an ectatic ascending aorta.*

Algorithm 1 Robust Stroke Volume Quantification

procedure ROBUST_SV
  $P \leftarrow$ quantification plane (Sec. 5.1)
  $A \leftarrow$ angulation samples (Sec. 5.3)
  for $i \leftarrow 0$ **to** size$(A) - 1$ **do**
    /*normal*/ $P.\vec{n} \leftarrow A_i$
    $P.\vec{n}_x$, $P.\vec{n}_y \leftarrow$ orthonormal system construction
    /*scale*/ $P.\vec{s} \leftarrow$ fit P to vessel mesh (Sec. 5.1)
    GPU buffer $\leftarrow$ add parameters of current P
  $F \leftarrow$ FLOWRATES_GPU() // one shader per angulation
  $SV \leftarrow$ stroke volumes
  for $i \leftarrow 0$ **to** size$(A) - 1$ **do**
    $f \leftarrow$ time-resolved flow rates F_i for A_i
    $S \leftarrow$ periodic spline fitted to f
    $SV_i \leftarrow$ integral of S (Fig. 2c)
  return median of SV

procedure FLOWRATES_GPU() (Sec. 5.2)
  $P \leftarrow$ current quantification plane configuration
  $\mathbb{V} \leftarrow$ flow field
  $T \leftarrow$ number of temporal positions
  $fr \leftarrow$ flow rate vector of size T
  for $x \leftarrow 0$ **to** /*grid size x*/ $P.g_x - 1$ **do**
    for $y \leftarrow 0$ **to** /*grid size y*/ $P.g_y - 1$ **do**
      $\vec{w} \leftarrow (x, y)$ to world coordinates (Sec. 5.1)
      if $\vec{w}$ in binary vessel segmentation **then**
        for $t \leftarrow 0$ **to** $T - 1$ **do**
          $\vec{u} \leftarrow \mathbb{V}(\vec{w}, t)$ (Sec. 3.3)
          $fr_t \leftarrow fr_t + \vec{u} \cdot P.\vec{n}$ (Sec. 5.2)
  for $t \leftarrow 0$ **to** $T - 1$ **do**
    $fr_t \leftarrow fr_t \cdot (P.s_x \cdot P.s_y)$ // area per rectangle in grid
  return fr

able to produce this behavior. Instead, physiologically implausible local SV minima and maxima occur. Therefore, we describe a method to fit a function to the SVs along the centerline that meets the experts' expectations.

The robust SV determination is performed for each of the equidistant centerline points. The x-axis in Figure 3 describes the centerline points in flow direction so that the left part of the plot corresponds to the approximate valve location. The yellow boxes show the interquartile ranges (IQR), which are the middle 50% of the sorted SV samples. Large ranges indicate high sensitivity to the angulation and thus uncertainty in the corresponding vessel section. The thin blue curve interpolates the medians.

The expected continuous SV decrease along the centerline is enforced by fitting each one monotonous function to the partial functions left and right of the peak median SV, which is determined for this purpose. In our implementation this non-trivial task is realized with an iterative cubic spline fitting[¶], where the parameter $\rho \in [-15, 15]$ controls a non-

¶ spline1dfitpenalized (ALGLIB)

linearity penalization. High and low ρ lead to linear least squares approximation and interpolation, respectively. Our procedure is initialized with $\rho = -5$. After the spline is fitted, its monotonicity is determined by evaluating the signs of all first derivatives. If it is not monotonous, ρ is slightly increased by 0.1, otherwise the loop stops.
Unfortunately, C^0-continuity of the two fitted monotonous functions is not guaranteed. As a remedy to remove the small gap, both functions are concatenated and smoothed in experimentally determined 15 iterations using a one-dimensional binomial filter with kernel size 5. Figure 3 shows the resulting function in red.

5.5. Robust Regurgitation Fraction Quantification

The described robust SV determination can be adopted for RF quantification. This requires the antegrade (AFV) and retrograde flow volume (RFV). To calculate them, the flow rate $fr(t)$ is separated into forward flow $fr^+(t)$ and backward flow $fr^-(t)$. When the flow rates per rectangular grid element of a plane are accumulated (recall Algorithm 1), $fr^+(t)$ and $fr^-(t)$ consider only positive and negative flow rates, respectively. Like the integral of the flow rate $fr(t)$ is the SV, the integrals of $fr^+(t)$ and $fr^-(t)$ provide the AFV and RFV. Partially monotonous functions are fitted in the same manner as for the SV. The tasks are independent from one another and thus can be performed in parallel threads on the CPU. The RF is then obtained as $\mathrm{RFV}/(\mathrm{AFV}+\mathrm{RFV})$. Figure 3 shows the resulting AFV (green) and RFV (orange) functions.

6. Results

This section contains a qualitative evaluation based on selected datasets, an evaluation of the quantification plane parameters and a subsequent discussion.

6.1. Qualitative Evaluation

We present five selected, anonymized datasets of the aorta that were discussed with each two collaborating radiologists and cardiologists. The evaluation was performed informally, i.e., no specific tasks had to be solved. The robust SV and RF quantification for the whole centerline as well as partially monotonous function fitting took about 25 seconds on average per dataset on a GeForce GTX 680 and Intel i7-3930K. The employed default parameters are discussed in Section 6.2. All images were directly captured from our developed software, which is used by our clinical collaborators for research purposes.

6.1.1. Healthy Volunteer

The first dataset shows a healthy volunteer. Figure 4a illustrates the result of our automatic quantification procedure. The highest SV deviations and thus sensitivity to different plane angulations are located at the beginning of the aortic arch. The experts assume this might be due to the physiological helix that occurs during systole. Regions with laminar flow seem to be less susceptible. The SVs show a physiologically implausible local minimum at about one third of the centerline, where the aortic arch ends. A possible explanation is a small segmentation error. The vessel diameter in and after the aortic arch is 1.5 cm but decreases to 1.24 cm at the transition. Figure 4c shows the systolic flow and a quantification plane close to the valve, where our method determined 82.03 ml peak SV. A RF of 0.51% at this position indicates a properly functioning aortic valve.

6.1.2. BAV Patient with Dilated Ascending Aorta

This patient has a bicuspid aortic valve (BAV). The upper diagram in Figure 4b shows the SVs along the centerline obtained with conventional quantification. A nearly vanishing value at the beginning is conspicuous. Qualitative flow analysis reveals prominent systolic vortex flow in the abnormally widened ascending aorta. This is likely the cause for the enormous SV deviation in this vessel section. Nevertheless, our robust SV procedure resolved the vanishing, as shown in the lower diagram of Figure 4b. Figure 4d shows the systolic vortex flow and the location of the plane where 102.5 ml peak SV were determined. Contrary to the employed heuristic, this is not located directly above the valve but rather at the end of the vortex.
The conventionally quantified RF ranges from 3% to 47%. The experts did agree on an increased amount of retrograde flow, but struggled to specify a concrete value. Our method determined 7.32% RF, which led to rejection of a valve replacement surgery as reasonable treatment option.
Figure 3 shows a similar patient with vortex flow in the ectatic ascending aorta. The same high sensitivity to different plane angulations is observable.

6.1.3. Coarctation Patient

The next patient has a coarctation. Qualitative flow analysis shows three systolic vortices: a slight helix above the aortic valve, a small vortex before the narrowing and one large helix in the post-stenotic vessel section, illustrated in Figure 5c. Figure 5a shows the SV deviations along the centerline. There is a local SV minimum in the coarctation at about one third of the centerline, which again is considered as physiologically implausible. In addition to potential segmentation inaccuracies like in the healthy volunteer, this might be due to the low data resolution. The vessel diameter shrinks about 50% in the narrowed region. Consequently, it is represented by far less voxels, which enhances partial volume effects.
The highest SV deviations occur in the post-stenotic vessel section, approximately in the middle of the centerline, where the largest vortex is present. The collaborating experts agree that this is the likely cause for the quantification uncertainties. In contrast to the previous BAV patient, the 140.75 ml peak SV is located close to the aortic valve despite of the slight helix.

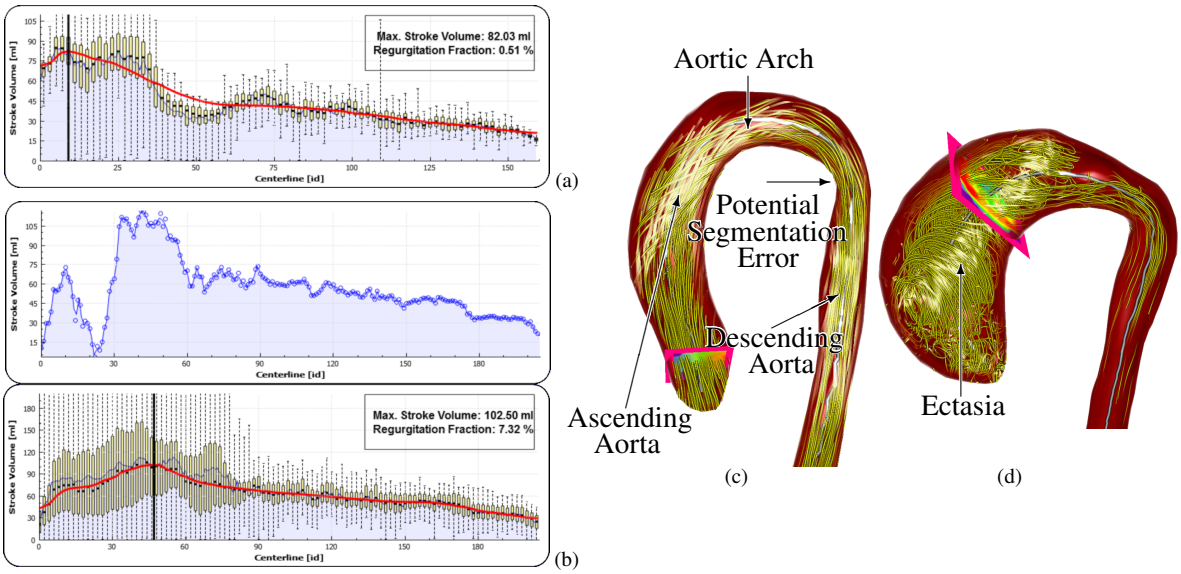

Figure 4: *(a, c) The plane with the maximal SV is located near the aortic valve in this healthy volunteer. A local SV minimum at the end of the aortic arch might be due to a potential segmentation inaccuracy. (b, d) A large systolic vortex in the dilated ascending aorta of this BAV patient causes high SV deviations and that the peak SV is not located directly above the valve. The upper diagram shows the physiologically implausible result of the conventional quantification method. The large SV gap in the ascending aorta does not occur in the result of our robust procedure.*

6.1.4. Bypass Patient

A bypass surgery was performed to treat this patient's former coarctation. The altered vessel shape promotes the formation of systolic vortex flow in the ascending aorta, shown in Figure 5d. The obtained SV deviations are presented in Figure 5b. The SV peak is located close to the valve despite of the slight helix, like in the previous patient. Moreover, a high number of local SV minima and maxima is noticeable. The numbers 1 to 6 help to connect the diagram with centerline positions. The minima correspond to curved vessel sections, whereas the maxima are located at the straight regions in between. A possible explanation is that partial volume effects make it difficult to capture the quickly changing flow directions in curved vessel sections. However, our partially monotonous function fitting produces a physiologically plausible SV development along the centerline.

6.2. Sample Generation Parameter Evaluation

Reasonable default values make the specification of unintuitive parameters unnecessary and thus increase the practical applicability of our method. We experimentally determined a well-functioning standard configuration during the development process, which is a grid size of $\vec{g} = 50 \times 50$ (recall Section 5.1), an angulation tolerance $\alpha = \pi/4 \mathrel{\widehat{=}} 45^{\text{o}}$ and Poisson-distributed angulation samples with a minimum distance of $d_{\text{min}} = 0.075$ on the unit sphere surface (recall Section 5.3). The validation of these parameters is shown exemplary for the peak SV of the BAV patient (see Section 6.1.2), which represents our experiences for all datasets.

New angulation samples are generated for each calculation. Thus, every plane evaluation is repeated 100 times per parameter set, resulting in a series of SVs. The defaults produce 102.5 ± 0.65 ml, which is the median of the samples plus minus half of the IQR (recall Section 5.4).

Modifications of α produced 109.67 ± 0.95 ml for 15^{o}, 107.25 ± 1.01 ml for 30^{o}, 102.5 ± 0.65 ml for the default 45^{o}, 102.28 ± 0.65 ml for 60^{o}, 112.79 ± 0.88 ml for 75^{o} and 122.4 ± 0.82 ml for 90^{o} The IQRs were lowest for 45^{o} and 60^{o} and the best agreement with 105 ml SV estimated by the experts was achieved with $\alpha \in [30^{\text{o}}, 60^{\text{o}}]$. As a consequence, $\alpha = \pi/4 = 45^{\text{o}}$, the middle of this range, seems appropriate as default value.

Altered grid sizes produced 97.39 ± 0.4 ml for 5×5, 102.39 ± 1.14 ml for 25×25, 102.5 ± 0.65 ml for the default 50×50, 102.32 ± 0.27 ml for 75×75 and 101.43 ± 0.69 ml for 100×100. There were no significant changes above grid sizes of 25×25. Though, planes that are fitted to large aneurysms with, e.g., 55mm vessel diameter have isotropic rectangle sizes of $55/25 = 2.2$ mm in 25×25 grids. To ensure that the rectangles are smaller than our data's finest resolution of 1.77 mm in one dimension, we use 50×50 grids as default.

Altered d_{min} of the Poisson-distribution produce 103.87 ± 2.13 ml for 0.165 ($\approx$50 samples), 102.31 ± 1.13 ml for 0.1 ($\approx$125 samples), 102.5 ± 0.65 ml for the default 0.075 ($\approx$200 samples) and 101.65 ± 0.48 ml for 0.05 ($\approx$500 samples). Standard uniform distribution (recall Section 5.3) produces 104.96 ± 8.09 ml for 50 samples, 102.84 ± 4.78 ml for 125 samples, 103.07 ± 3.98 ml for 200 samples and

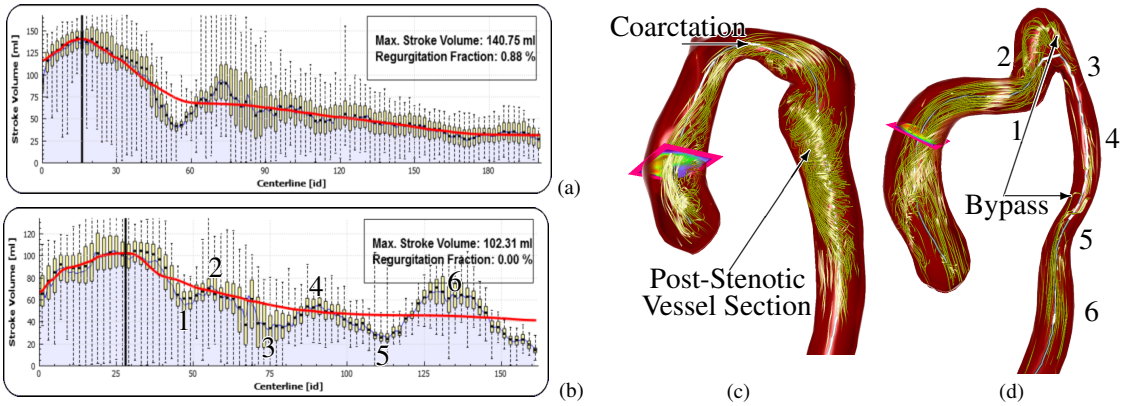

Figure 5: *The SV peaks in both patients are located close to the valves despite of slight systolic helices. (a, c) A local SV minimum occurs in the patient's coarctation. The post-stenotic region shows the highest SV deviations probably due to the large systolic helix. (b, d) Numerous local SV minima are located in bent vessel sections of this patient with a bypass.*

101.12 ± 2.38 ml for 500 samples. The IQRs from Poisson-distribution are significantly lower than from uniform distribution. It was below 1 ml for $d_{\min} = 0.075$ and reduced only marginally with more samples. The difference between both distributions decreases with an increasing number of samples. However, Poisson-distribution requires fewer samples to achieve sufficient results. The higher costs for angulation generation are not substantial. Summarizing, the sample distribution has the highest influence on the results.

6.3. Discussion

The presented robust SV and RF quantification does not require user-defined parameters. Instead, the user's only responsibility is to generate a valid segmentation and centerline. The automatically obtained SV peak values show good correspondence with the expected results estimated by our collaborating experts with conventional methods.

Uncertainties, i.e. the sensitivity to different plane angulations, were visualized with box plots. Especially prominent vortex flow seems to cause high uncertainties since corresponding vessel sections show large interquartile SV ranges. High variations led to careful result interpretation, whereas small deviations created trust.

Contrary to the assumptions, the SV peaks were not always located directly above the valve. This is a serious error potential for the common 2D PC-MRI standard in addition to the plane angulation that is required before the acquisition.

Our robust SV determination compensated errors that occur with conventional quantification due to low data resolution and segmentation errors. The partially monotonous function fitting was able to generate physiologically plausible SV developments along the vessel course. The application of our method to retrograde and antegrade flow volumes enabled to robustly determine RFs even when conventional methods did not allow reliable assessment. This is of particular importance for the discussion of appropriate treatments.

The parameter evaluation showed that the angulation sample distribution has the highest influence result robustness. Poisson-distributed angulation samples were determined as most appropriate.

7. Conclusion and Future Work

We presented a method to robustly determine the SV and RF in cardiac 4D PC-MRI data. The procedure was developed in close collaboration with cardiologists and radiologists and represents an automatization of their manual approach. Statistical information were presented as box plots to convey uncertainties. The experts' expectations were employed as heuristics to establish a procedure that creates physiologically plausible SV developments along the vessel course. The GPU's computing power was exploited to achieve average calculation times of 25 seconds.

In addition to segmentation inaccuracies and partial volume effects, prominent vortex flow was identified as main cause for uncertainties. Against the assumption, the SV peaks were not in all cases directly located above the valve. This is an additional error potential for the current 2D PC-MRI standard since the default is to use a plane above the valve that is orthogonal to the vessel's centerline.

Due to reasonable default parameters the only required user input is a vessel segmentation and centerline, which both exploit expert knowledge. Hence, our procedure is eligible to be part of an automatic data evaluation procedure in the future that supports clinical report generation.

Until now, SV and RF quantification requires knowledge of highly specialized experts on the cardiovascular system and its hemodynamics. Our method reduces this to mainly anatomical knowledge. However, the newly enabled uncertainty assessment still needs experience. More sophisticated visualizations might support the interpretation in the future.

Our presented procedure handles one linear centerline. For branching vessels, such as the pulmonary artery, this means that only one path can be evaluated at a time. The corresponding algorithm extension to branching centerlines is future work.

Acknowledgements

We would like to thank Matthias Grothoff and Franziska Reinhold for fruitful discussions.

References

[AEIR03] ANTIGA L., ENE-IORDACHE B., REMUZZI A.: Centerline Computation and Geometric Analysis of Branching Tubular Surfaces with Application to Blood Vessel Modeling. In *Proc Winter School Comput Graph (WSCG)* (2003). 3

[BMGS13] BORN S., MARKL M., GUTBERLET M., SCHEUERMANN G.: Illustrative Visualization of Cardiac and Aortic Blood Flow from 4D MRI Data. In *IEEE PacificVis* (2013), pp. 129 – 136. 2

[BPM*13] BORN S., PFEIFLE M., MARKL M., GUTBERLET M., SCHEUERMANN G.: Visual Analysis of Cardiac 4D MRI Blood Flow Using Line Predicates. *IEEE Trans Vis Comput Graph 19* (2013), 900 – 912. 2

[CBHP14] CARNECKY R., BRUNNER T. BORN S. W. J., HEINE C., PEIKERT R.: Vortex Detection in 4D MRI Data: Using the Proper Orthogonal Decomposition for Improved Noise-Robustness. In *Proc. EuroVis* (2014), p. to appear. 2

[CTK*11] CARLSSON M., TÖGER J., KANSKI M., MARKENROTH BLOCH K., STÅ HLBERG F., HEIBERG E., ARHEDEN H.: Quantification And Visualization of Cardiovascular 4D Velocity Mapping Accelerated with Parallel Imaging or k-t BLAST: Head to Head Comparison And Validation at 1.5 T and 3 T. 2

[DP80] DORMAND J. R., PRINCE P. J.: A Family of Embedded Runge-Kutta Formulae. *J Comput Appl Math 6* (1980), 19 – 26. 3

[DR04] DÌAZ C., ROBLES L. A.: Fast Noncontinuous Path Phase-Unwrapping Algorithm based on Gradients and Mask. In *Proc Iberoameric Cong Patt Recog (CIARP)* (2004), pp. 116 – 123. 3

[FSS*12] FRANCOIS C., SRINIVASAN S., SCHIEBLER M., REEDER S., NIESPODZANY E., LANDGRAF B., WIEBEN O., FRYDRYCHOWICZ A.: 4D Cardiovascular Magnetic Resonance Velocity Mapping of Alterations of Right Heart Flow Patterns and Main Pulmonary Artery Hemodynamics in Tetralogy of Fallot. *J Cardiovasc Magn Reson 14*, 1 (2012), 16. 2

[GNBP11] GASTEIGER R., NEUGEBAUER M., BEUING O., PREIM B.: The FLOWLENS: A Focus-and-Context Visualization Approach for Exploration of Blood Flow in Cerebral Aneurysms. *IEEE Trans Vis Comput Graph 17*, 12 (2011), 2183 – 2192. 2

[HFS*11] HENNEMUTH A., FRIMAN O., SCHUMANN C., BOCK J., DREXL J., HUELLEBRAND M., MARKL M., PEITGEN H.-O.: Fast Interactive Exploration of 4D MRI Flow Data. *Proc of SPIE Med Imag 7964* (2011). 2

[HGH*10] HUMMEL M., GARTH C., HAMANN B., HAGEN H., JOY K.: IRIS: Illustrative Rendering for Integral Surfaces. *IEEE Trans Vis Comput Graph 16*, 6 (2010), 1319 – 1328. 2

[Hop99] HOPPE H.: New Quadric Metric for Simplifying Meshes with Appearance Attributes. In *Proc IEEE Vis* (1999), pp. 59 – 66. 3

[HSD13] HOPE M. D., SEDLIC T., DYVERFELDT P.: Cardiothoracic Magnetic Resonance Flow Imaging. *J Thorac Imaging 28*, 4 (2013), 217 – 230. 1, 2

[HWS*12] HOPE M. D., WRENN J., SIGOVAN M., FOSTER E., TSENG E. E., SALONER D.: Imaging Biomarkers of Aortic Disease - Increased Growth Rates with Eccentric Systolic Flow. *J Amer Coll Cardiol 60*, 4 (2012), 356 – 357. 2, 3

[JSH12] JAMRIŠKA O., SÝKORA D., HORNUNG A.: Cache-Efficient Graph Cuts on Structured Grids. In *Proc IEEE Comput Vis Patt Recog* (2012), pp. 3673 – 3680. 3

[KGP*13] KÖHLER B., GASTEIGER R., PREIM U., THEISEL H., GUTBERLET M., PREIM B.: Semi-Automatic Vortex Extraction in 4D PC-MRI Cardiac Blood Flow Data Using Line Predicates. *IEEE Trans Vis Comput Graph 19*, 12 (2013), 2773 – 2782. 1, 2, 3

[LHM*05] LANKHAAR J.-W., HOFMAN M. B. M., MARCUS J. T., ZWANENBURG J. J. M., FAES T. J. C., VONK-NOORDEGRAAF A.: Correction of Phase Offset Errors in Main Pulmonary Artery Flow Quantification. *J Magn Reson Imag 22*, 1 (2005), 73 – 79. 3

[LS10] LIU J., SUN J.: Parallel Graph-Cuts by Adaptive Bottom-Up Merging. In *Proc IEEE Comput Vis Patt Recog* (2010), pp. 2181 – 2188. 3

[MFK*12] MARKL M., FRYDRYCHOWICZ A., KOZERKE S., HOPE M. D., WIEBEN O.: 4D Flow MRI. *J Magn Reson Imag 36*, 5 (2012), 1015 – 1036. 1, 2

[MLP*10] MCLOUGHLIN T., LARAMEE R. S., PEIKERT R., POST F. H., CHEN M.: Over Two Decades of Integration-Based, Geometric Flow. *Comp Graph Forum 29*, 6 (2010), 1807 – 1829. 2

[MPN11] MENDIS S., PUSKA P., NORRVING B.: *Global Atlas on Cardiovascular Disease Prevention and Control*. World Health Organization, World Heart Federation and World Stroke Organization, 2011. 1, 2

[NJB*11] NEUGEBAUER M., JANIGA G., BEUING O., SKALEJ M., PREIM B.: Anatomy-Guided Multi-Level Exploration of Blood Flow in Cerebral Aneurysms. *Comp Graph Forum 30*, 3 (2011), 1041 – 1050. 2

[PCM*14] POTTERS W. V., CIBIS M., MARQUERING H. A., VANBAVEL E., GIJSEN F., WENTZEL J. J., NEDERVEEN A. J.: 4D MRI-Based Wall Shear Stress Quantification in the Carotid Bifurcation: A Validation Study in Volunteers Using Computational Fluid Dynamics. *J Cardiovasc Magn Reson 16*, Suppl 1 (2014), P162. 2

[PHL*13] PREIM U., HAUSE F., LEHMKUHL L., PREIM B., GREISER A., GROTHOFF M., GUTBERLET M.: Comparison of 4D and 2D Phase Contrast Magnetic Resonance Imaging of the Great Mediastinal Vessels. *J Cardiovasc Magn Reson 15*, Suppl 1 (2013), P35. 2

[TZG96] TAUBIN G., ZHANG T., GOLUB G.: Optimal Surface Smoothing as Filter Design. In *Proc Europ Conf Comput Vis*. 1996, pp. 283 – 292. 3

[vOPN*14] VAN OOIJ P., POTTERS W. V., NEDERVEEN A. J., COLLINS J. D., CARR J. C., MALAISRIE S. C., MARKL M., BARKER A. J.: Thoracic Aortic Wall Shear Stress Atlases in Patients with Bicuspid Aortic Valves. *J Cardiovasc Magn Reson 16*, Suppl 1 (2014), P161. 2

[vPBB*10] VAN PELT R., BESCOS J. O., BREEUWER M., C. R. E., GRÖLLER M. E., TER HAAR ROMENIJ B., VILANOVA A.: Exploration of 4D MRI Blood Flow Using Stylistic Visualization. *IEEE Trans Vis Comput Graph 16*, 6 (2010), 1339 – 1347. 2

[WKS*09] WÖHRLE J., KOCHS M., SPIESS J., NUSSER T., HOMBACH V., MERKLE N.: Impact of Percutaneous Device Implantation for Closure of Patent Foramen Ovale on Valve Insufficiencies. *Circulation 119*, 23 (2009), 3002 – 3008. 3